Influence of Rhenium on the Grain Boundary Strength, Phase Evolution, and High Temperature Mechanical Properties of a Fine-Grain Nickel-Base Superalloy at 982°C

Jian-Hong Liao[1,*], Hui-Yun Bor[2], Chuen-Guang Chao[1] and Tzeng-Feng Liu[1]

[1]*Department of Materials Science and Engineering, National Chiao-Tung University, 1001 Ta-Hsueh Road, Hsin-Chu 30049, Taiwan, R. O. China*
[2]*Materials and Electro-Optics Research Division, Chung-Shan Institute of Science and Technology, Lung-Tan, Tao-Yuan, 32599, Taiwan, R. O. China*

The influence of Re on the grain boundary (GB) strength, phase evolution, and 982°C mechanical properties of fine-grain Mar-M247 superalloy was investigated. Quantitative statistical analysis showed that an increase of Re content in Mar-M247 resulted in a decrease of the size, and an increase in the number of GB carbides. The results of tensile and 982°C/200 MPa creep tests showed that tensile properties and creep life both increase with an increase in Re up to a maximum at 3 mass%. The tensile and GB strength increased with increasing the number of fine GB carbides. The addition of 1~3 mass% Re reduced steady-state creep rates and postponed the onset of the acceleration stage in three ways: (1) by increasing the amount of primary cuboidal γ' phase; (2) by increasing the strength of γ matrix; and (3) by increasing the development of γ' raft. It also prolonged the duration of the accelerating creep stage by refinement and an increase in the number of GB carbides. The above mentioned factors resulted in a prolongation of creep life. It is noted that the GB carbide evolution and GB strengthening effect by addition of Re have not been reported in the nickel-base superalloy before. However, addition of greater amounts of Re, such as 5 mass% Re, causes deterioration of the tensile and creep properties due to the formation of P phases. [doi:10.2320/matertrans.M2011136]

1. Introduction

Mar-M247 Ni-base superalloy has been widely employed in fabricating advanced turbine blades and rotating parts in the aerospace industry because of its excellent castability and high temperature properties.[1–3] Because the fine-grain microstructure has advantages such as refined grains, carbides and precipitates, the fine-grain process was developed to improve the strength, creep and fatigue life of integral casting working at intermediate temperature (427~760°C).[4,5] Due to superior alloy design and control of the microstructure of Mar-M247, the fine-grain integral casting of this material has been applied at temperatures of up to 982°C.[6] Basically, Mar-M247 consists of 60–65% volume fraction of the reinforcing precipitates γ' in a face-centered cubic (FCC) γ matrix.[2,3]

In modern Ni-base superalloys, the γ' phase is limited to approximately 65–70% volume fraction to maximize precipitation hardening;[7,8] hence, the volume fraction of γ' in Mar-M247 is nearly at its limit. Strengthening the solid solution of the γ matrix is one way to further improve the strength of this alloy. On the other hand, the reliability of γ' at elevated temperatures is another concern for Mar-M247, because the growth of γ' significantly degrades creep life. The addition of slow diffusing elements into the alloy to prevent the γ' coarsing is thought to be a desirable solution to overcome these detrimental effects. Additionally, the GB strength declines drastically at high temperatures (above 760°C). Therefore, the carbides precipitating at the GB play an important role in the strengthening of GB at high temperature. Through the inhibition of GB sliding,

GB carbides contribute to an increase in strength and ductility.[1–3]

Current single crystal Ni-base superalloys are heavily alloyed with Re, resulting in increased strength and creep resistance, due to solid solution strengthening and the prevention of γ' coarsening during thermal exposure.[9–14] The incorporation of higher Re content is restricted by the formation of topological closed-packed (TCP) phases, such as σ, P, μ, and R.[15–18] Formation of a brittle TCP phase is often associated with the deterioration of tensile strength and creep damage.[19,20] To prevent the formation of a TCP phase, controlling the content of Re is an important consideration in the design of superalloys.

Until now, studies have focused on adding Re to single crystal Ni-base superalloys, and the resulting behavior at high temperatures. However, few studies have reported on the effects of adding Re to fine-grain superalloys. The purpose of this investigation was to determine the influence of Re on the mechanical properties of fine-grain Mar-M247 superalloy at 982°C.

2. Experimental

The Mar-M247 ingot used in this study was procured from a single master heat. 0, 1, 3, and 5 mass% Re were added to Mar-M247 and named as A, B(1Re), C(3Re), and D(5Re), respectively. Re was added to Mar-M247 ingot by melting in a vacuum furnace and then pouring into invest-ment cluster molds, to obtain cast rods using the Microcast-X technique. Microcast-X, developed by Howmet Corporation, is a fine-grain technique with controlled low super-heat and a high heat extraction rate.[5,17] The pouring and mold temperatures were 1380°C and 1100°C, respectively.

Table 1   The chemical compositions of superalloys investigated (mass%).

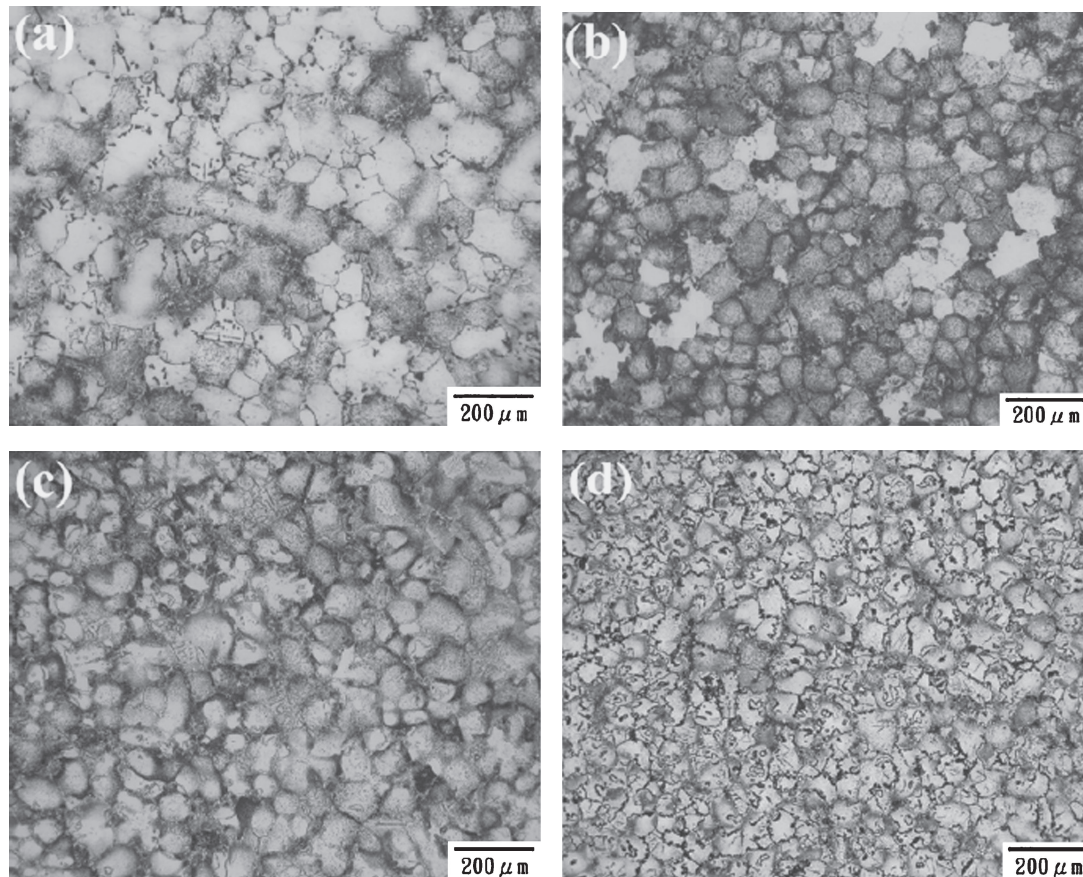| Alloy	Re	Cr	Co	Mo	W	Ta	Al	Ti	Hf	C	B	Zr	Ni
A(0Re)	—	8.35	10.10	0.69	9.91	3.05	5.42	1.00	1.32	0.15	0.02	0.04	bal.
B(1Re)	0.97	8.41	9.98	0.69	10.02	2.99	5.38	0.98	1.22	0.14	0.02	0.04	bal.
C(3Re)	2.92	8.42	9.99	0.69	10.02	3.01	5.33	0.98	1.29	0.14	0.02	0.04	bal.
D(5Re)	4.99	8.40	10.00	0.70	10.03	2.99	5.37	0.97	1.22	0.14	0.02	0.04	bal.

Fig. 1   OM images of alloys (a) A, (b) B(1Re), (c) C(3Re), and (d) D(5Re) after heat treatment.

Table 1 lists the nominal chemical composition of the resulting alloys. The chemical composition of the each alloy was determined using X-ray fluorescence, with the exception of Re content, which was determined by inductive coupled plasma chemical analysis. Hot-isostatic press (HIP) was utilized in this study to eliminate casting pore that was one possible factor influencing the results of tensile and creep tests. HIP and heat treatment conditions were conducted according to Ref. 3). The HIP was applied for 4 h at 1185°C, under gaseous argon at a pressure of 172.4 MPa, followed by cooling under argon. Heat treatment of the solid solutions was carried out at 1185°C for 2 h under vacuum, followed by cooling under argon. Samples were subjected to aging heat treatment at 871°C for 20 h under vacuum conditions and then cooled to room temperature (RT) in the furnace.

The heat-treated cast rods of each alloy were machined into standard test bars with a gauge diameter of 6.3 mm and gauge length of 26 mm. Tensile tests were performed using an Instron 1125 universal test machine with 0.2 mm min^{-1} crosshead speed at RT, 760°C, and 982°C in atmosphere.

Creep tests were carried out using constant-load creep testing equipment at 982°C/200 MPa in atmosphere. Four tests were conducted for each tensile and creep test.

General metallographic samples were polished and etched using 10 mL HNO$_3$ + 5 mL HCl + 30 mL lactic acid. Grain size was measured by determining the mean linear intercept of the grains using optical microscopy (OM). A scanning electron microscope (SEM) equipped with energy dispersive spectroscopy (EDS) was used to characterize the microstructure. SEM images were obtained using the secondary electron mode at 20 kV. Transmission electron microscopy (TEM) was used to determine the crystal structure of the TCP phase. Twin jet electrolytic etching was employed in 90% CH$_3$COOH+10% HClO$_4$ solution to prepare TEM specimens. Quantitative statistical analyses of the GB carbide, including particle size and linear density, were measured from more than 400 carbides using an artificial calculation method based on SEM images. Fracture surfaces were characterized by SEM. Longitudinal section samples were metallographically prepared, as described above, and examined by SEM.
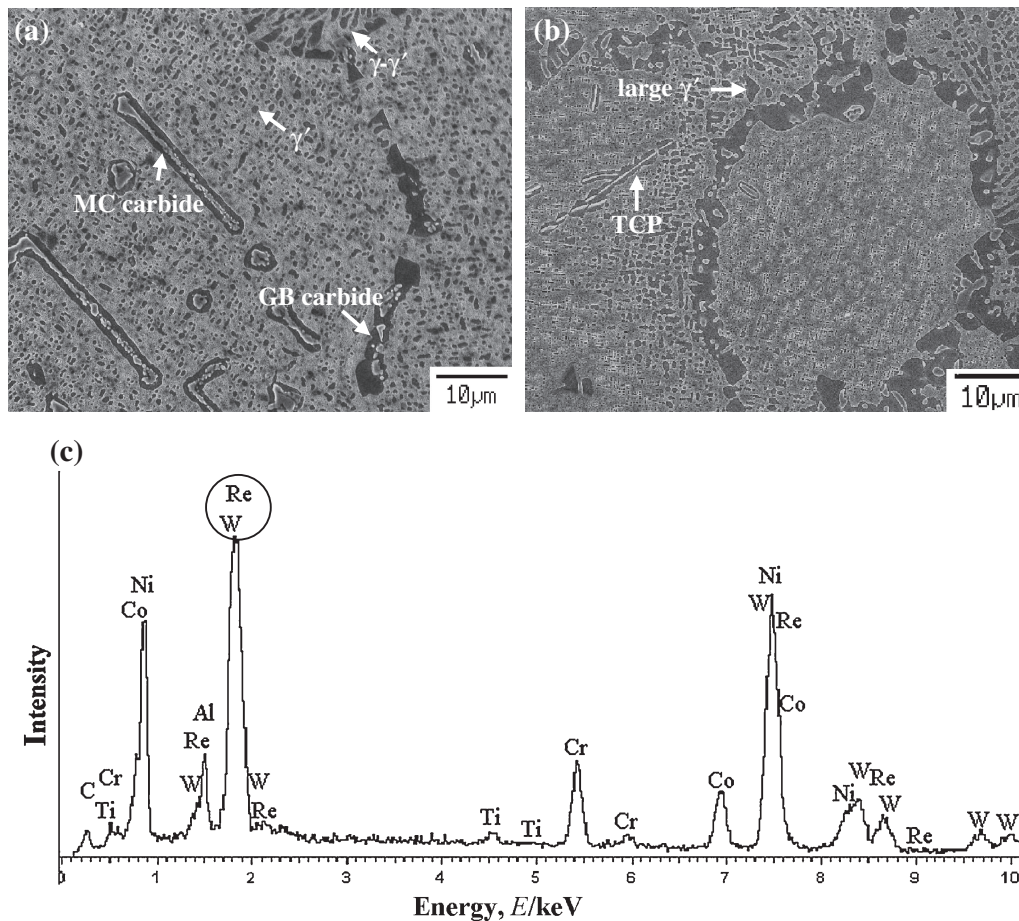
Fig. 2 SEM microstructure of alloys (a) A and (b) D(5Re) after heat treatment. (c) EDS spectra of TCP phase in alloy D(5Re).
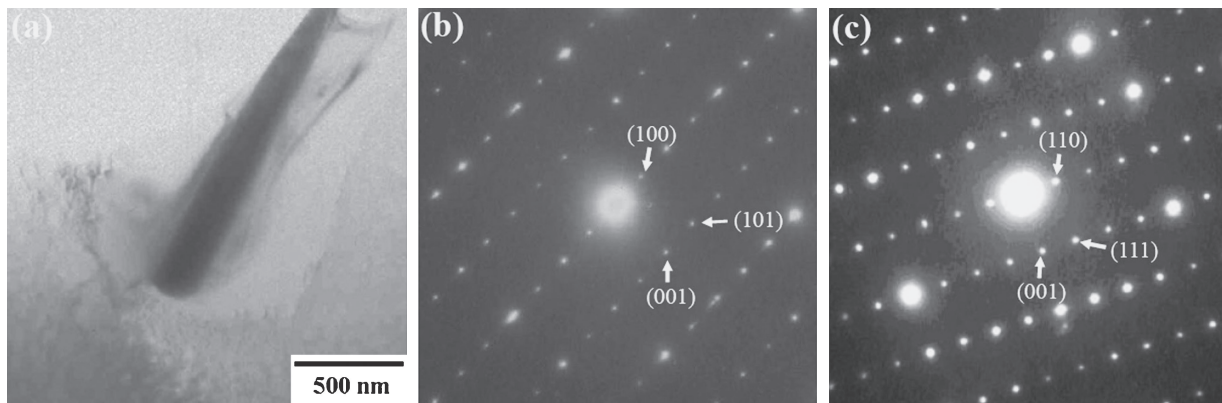

Fig. 3 The TEM (a) bright-field image of the P phase, (b) selected-area diffraction pattern (SADP) with [010] zone, and (c) [1$\bar{1}$0] zone.

3. Results

3.1 Microstructure and characteristics of GB carbide

Figure 1 displays the grain size of four alloys following heat treatment. The grain sizes of alloys refine from 90 to 50 μm with increasing Re content. Figure 2(a) shows the original Mar-M247 superalloy. The main phases comprise: (1) the γ matrix, (2) the reinforcing phase γ' homogeneously distributed throughout the γ matrix, (3) strip-like and blocky MC carbides within a grain interior, (4) particle and blocky carbides at the GB, and (5) a rosette structure of γ-γ' eutectic.

For alloys B(1Re) and C(3Re), the microstructure revealed similar characteristics to that of alloy A. Alloy D(5Re) exhibited inhomogeneously distributed γ' phase with fine cuboid shaped γ' particles in the core area of the grain and the large, block shaped γ' particles (1–3 μm in size) situated in the region near the GB (Fig. 2(b)). Needle-like 10–20 μm long TCP phases were observed within the grain interior in alloy D(5Re), and EDS measurements indicated that this phase had high Re and W content (Fig. 2(c)). Comparing the TEM analysis of the TCP phase (Fig. 3) with other reports,[15,18] the TCP is identified as P phase, with an

orthorhombic structure and lattice constant $a = 0.901$ nm, $b = 1.689$ nm, and $c = 0.471$ nm. Figures 4(a)–(c) illustrate the characteristic changes in GB carbides. For alloy A, carbide size ranged from 0.3 to 10 µm non-uniformly distributed along the GB. For alloys C(3Re) and D(5Re), the carbides become homogeneous and are more closely distributed in the GB with sizes ranging from 0.5 to 2 µm. The EDS measurements indicated that GB carbide of alloy

D(5Re) had high Re and W content (Fig. 4(d)). Quantitative statistical results concerning GB carbide characteristics in Mar-M247 superalloy with various proportions of Re are shown in Fig. 5. Figure 5(a) illustrates that the average particle size of GB carbide is reduced to 1.1 µm from 1.9 µm in the alloy A (i.e., the GB carbides are refined through the addition of Re). Figure 5(b) shows the linear density of GB carbides along the GB. It is obvious that the number of GB carbides increase with an increase in the addition of Re. This provides evidence that the addition of Re causes an increase in the distribution density. Figure 6 shows the highly magnified SEM morphology of γ' precipitates with two distinct sizes in the core area of grain. Two distinct sizes γ' phases (primary block γ' and secondary γ' phases) were distributed in the alloy A. The primary γ' phase becomes finer and more cuboidal with an increase in the content of Re. The sizes of primary block γ', primary cube γ', and secondary γ' were about 0.8, 0.3, and 0.05 µm, respectively. No obvious difference change in size occurred for secondary γ' phases in any of alloys.

3.2 Tensile and creep tests

Table 2 shows the tensile properties of Mar-M247 alloy with various Re contents at room and elevated temperatures. According to the results, the tensile properties of alloys exhibited a similar tendency at various temperatures. The ultimate tensile strength (*UTS*) and 0.2% offset yield strength (*YS*) increase with Re content up to a maximum of 3 mass%. The elongation (*EL*) was nearly invariable in alloys containing 0~3 mass% Re; however, C(5Re) displayed the lowest of *EL*.

Figure 7 illustrates the creep curves of Mar-M247 superalloy with various Re contents at 982°C/200 MPa condition. Table 3 lists the creep data. The creep curves of alloy A, B(1Re), and C(3Re) showed a steady-state creep stage, followed by an accelerating creep stage leading to failure; however, no primary creep stage was observed. On the other hand, there was no clear definition of steady-state creep regimes for alloy D(5Re); this alloy exhibited a continuing increase in creep rate until failure. According to the EMS-55447 specification,[21] the creep life of the Mar-M247 superalloy should be longer than 25 h and the *EL* must exceed 4% at 982°C/200 MPa. During service, turbine blades are usually strained below 1 or 2%, therefore the criterion time to reach 1% ($t_{1\%}$) or 2% ($t_{2\%}$) strain was chosen
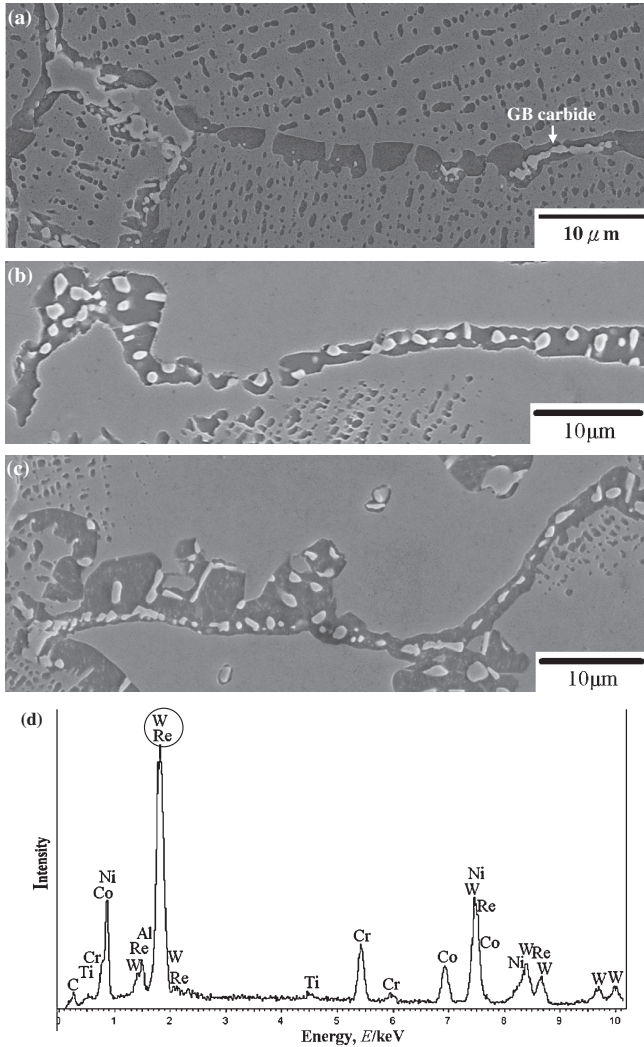

Fig. 4 The morphology of GB carbides in alloys of (a) A, (b) C(3Re), and (c) D(5Re); (d) EDS spectra of GB carbide in alloy D(5Re).
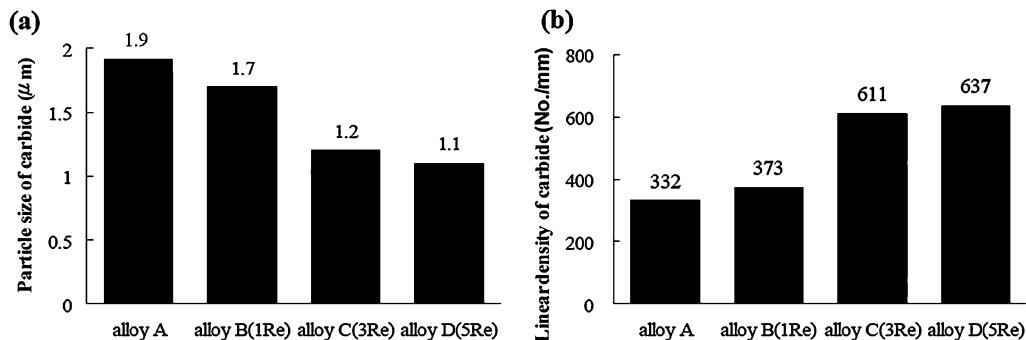

Fig. 5 Quantitative analysis results of GB carbide characteristics in Mar-M247 superalloys with various Re contents: (a) average particle size and (b) linear density of GB carbide.
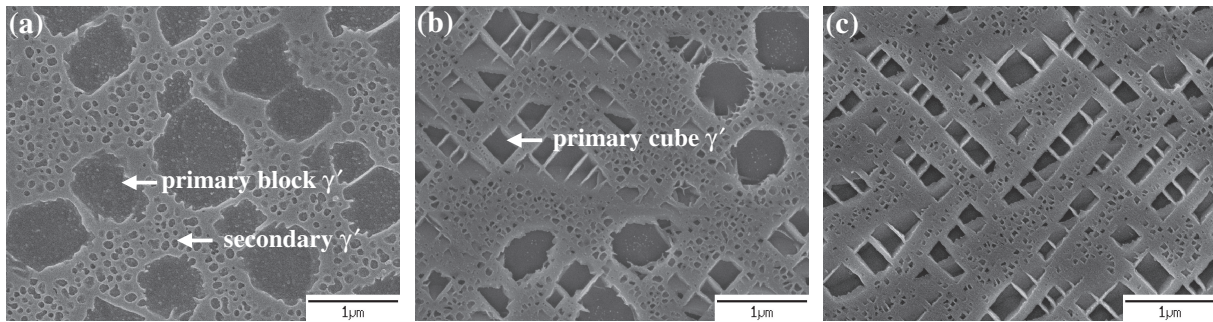
Fig. 6   The γ' phase morphology (in core area of grain) of alloys (a) A, (b) C(3Re), and (c) D(5Re) after heat treatment.

Table 2   Tensile test results at various temperatures.

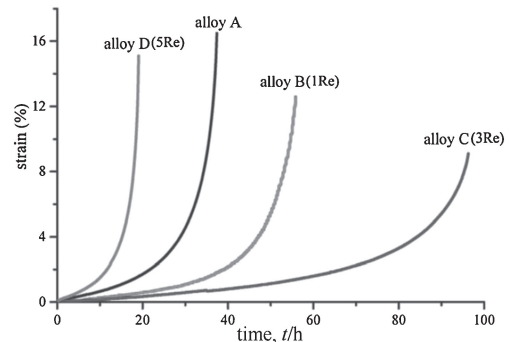| Temp.	Alloy	UTS (MPa)	YS (MPa)	EL (%)
RT	A(0Re)	1121–1139	967–987	4.8–6.0
	B(1Re)	1124–1143	973–995	4.7–6.2
	C(3Re)	1190–1217	1043–1074	4.0–6.0
	D(5Re)	1083–1108	932–968	1.3–3.0
760°C	A(0Re)	1146–1176	969–1013	4.4–6.0
	B(1Re)	1157–1183	985–1015	4.5–6.3
	C(3Re)	1228–1254	1066–1088	4.3–6.7
	D(5Re)	1071–1092	936–970	1.7–2.9
982°C	A(0Re)	590–613	436–458	6.4–7.5
	B(1Re)	599–625	457–476	6.2–7.1
	C(3Re)	628–646	494–518	5.5–6.2
	D(5Re)	558–581	435–456	2.5–3.6

Fig. 7   Creep curves of Mar-M247 superalloys with various Re contents tested under 982°C/200 MPa.

Table 3   Creep test results of Mar-M247 superalloys with various Re contents under 982°C/200 MPa.

	creep life (h)	EL (%)	[*1]$t_{1\%}$ (h)	[*1]$t_{2\%}$ (h)	[*1]steady-state creep rate (s^{-1})	[*1]period of steady-state creep (h)	[*2]period of accelerating creep (h)
EMS-55447	>25	>4	—	—	—	—	—
A(0Re)	34.4–46.2	11.4–16.4	14.2	21.7	19.45×10^{-8}	13.6	23.8
B(1Re)	55.8–69.7	11.1–14.4	29.1	39.0	9.54×10^{-8}	29.1	26.7
C(3Re)	81.9–96.3	9.6–14.1	46.4	66.6	5.98×10^{-8}	46.1	50.2
D(5Re)	11.1–19.1	10.5–14.7	7.7	11.6	—	—	19.1

[*1]The value is based on creep curves of Fig. 7.
[*2]The period of accelerating creep is defined as the time from the beginning of strain rate (the slope of creep curve) rise to the specimen fracture.

as a key indicator for creep strength.[3,12] Except for the alloy D(5Re), the creep life and *EL* of alloy A, B(1Re), and C(3Re) all exceed specification values. The $t_{1\%}$, $t_{2\%}$, period of steady-state, period of accelerating creep, and creep life increased with an increase in Re content, to a maximum at 3 mass%. In contrast to alloy A, the $t_{1\%}$, $t_{2\%}$, and creep life of alloy C(3Re) was prolonged by 3.3, 3.1, and 2–3 times, respectively. Finally, the creep properties of alloy D(5Re) decreased from the maximum values attained by the alloy C(3Re), showing the detrimental effect of excessive addition of Re in the alloy.

3.3 Fractographic observation and microstructural evolution

To investigate the effect of Re addition on fracture behavior during tensile and creep tests, we examined both the fracture surfaces and the longitudinal sections adjacent to the region of the fractures. Figure 8 shows the fractographs of 982°C tensile tests. From the fracture surface of alloy A, it is clear that crack mainly occurs along the GB (Fig. 8(a)). Figure 8(b) shows further evidence; a carbide film of approximately 1 μm in thickness presents at the fracture position of the GB, indicating a typical intergranular fracture. A similar fracture is seen in alloys B(1Re) and C(3Re), where crack occurs along the GB. The fracture surface of alloy D(5Re) illustrates that the crack is along the GB, and that a secondary crack occurs within the grain interior (Fig. 8(c)). Further examination of the longitudinal section shows that the crack is along the P/γ interface whilst the micro-cracks appear at the P phase (Fig. 8(d)). The dimensions of the needle-like P phase are very similar in size to the length of the secondary crack observed in Fig. 8(c). Obviously, another crack onset occurs at the P/γ interface and P phase.
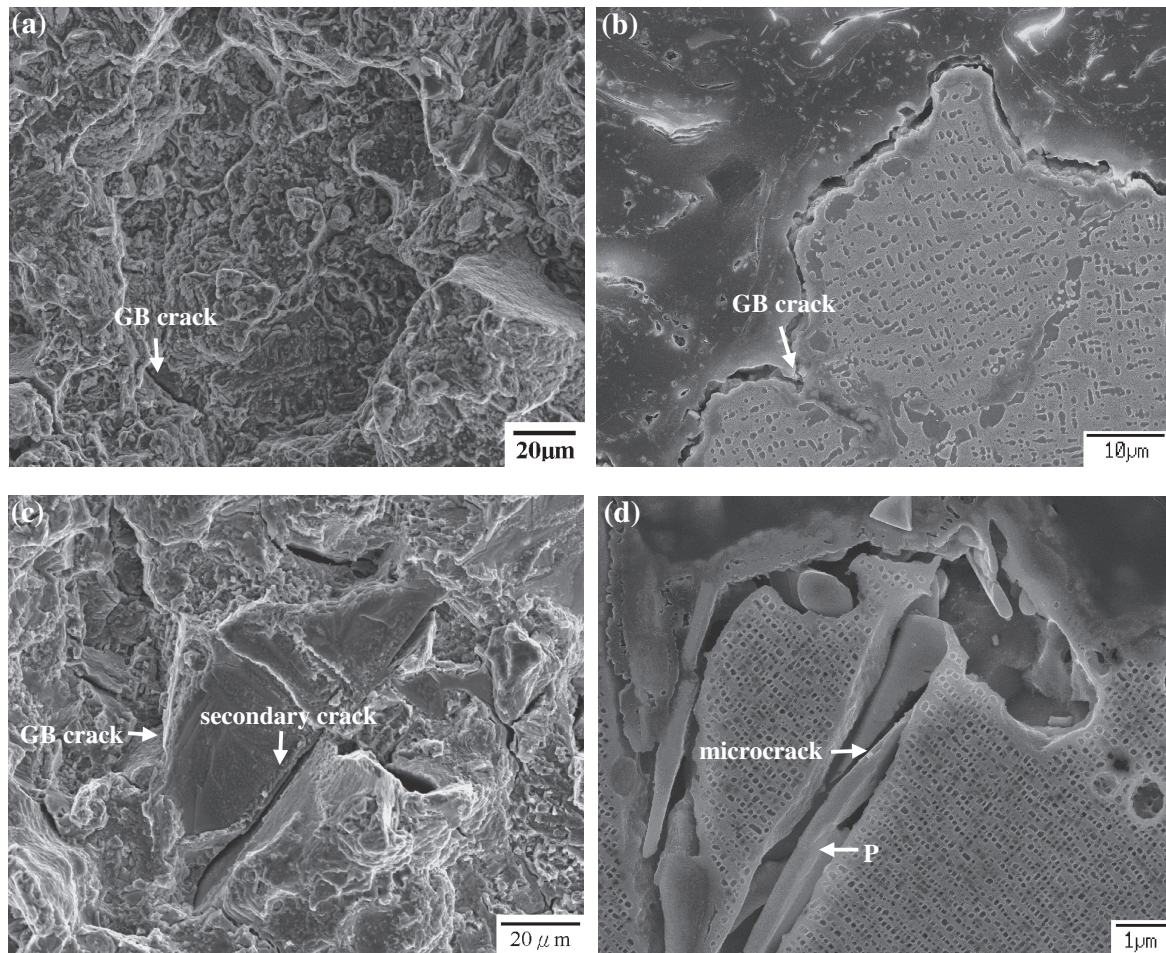
Fig. 8 SEM fractographs of 982°C tensile test: (a) fracture surface and (b) longitudinal section of alloy A; (c) fracture surface and (d) longitudinal section of alloy D(5Re).

In a comparison of the as-heated sample with the fractured sample, no microstructural evolution was observed in the tensile test. In tests of other temperatures, each alloy had the same fracture mode as in the 982°C tests.

For the 982°C/200 MPa creep tests, each alloy presented similar fracture behavior as those observed in the tensile test. The fracture surface and longitudinal section of alloy A show that cracks occur mainly along the GB, indicating a typical intergranular fracture (Figs. 9(a)–(b)). Similar fracture behavior is shown in alloys B(1Re) and C(3Re). For the fracture surface of alloy D(5Re), cracks were observed on the GB, and secondary cracks were observed within the grain interior (Fig. 9(c)). It is evident from Fig. 9(d) that the cracks occurred on the GB, and along the P/γ interfaces. The needle-like P phase showed similar dimensions to the secondary cracks observed in Fig. 9(c). Figures 10(a)–(c) show the γ' rafting microstructure in creep failure samples. The primary γ' phase has directionally coarsened into rafts in the direction perpendicular to the stress axis. No secondary γ' phase was observed. The alloy A exhibited γ' rafts with varying levels of development and thickness, and finer γ' tended to raft better than coarse γ'. On the other hand, except for the large γ' phases existing near the GB exhibited a immature γ' raft morphology in alloy D(5Re), a higher Re content alloy exhibited a finer and more uniform thickness in

the γ' raft. As Re content increases, average γ' raft spacing decreases from 0.3 to 0.15 µm. To study the evolution of γ' precipitates, the test was interrupted at creep for 10 h. Figure 10(d) provides evidence that the well-developed γ' rafts have already formed at early stages of creep in the core area of the grains in alloy D(5Re).

4. Discussion

4.1 Effect of Re on tensile properties

Generally, the refinement of γ' size is beneficial to tensile strength. Studies have reported that the large atomic radius of Re partitioned mainly to the γ matrix increases the γ/γ' lattice misfit, improving the strength of γ matrix.[7,10] According to the fractographic analysis, intergranular fracture exists in 0~3% mass Re-containing alloys, indicating the GB strength dominates the tensile strength and fracture behavior over other factors (γ' size or strength of γ matrix). Generally, GB strength is related to grain size and GB carbide. Except for high temperatures (over the half of melting temperature), a reduction in grain size is beneficial to GB strength.[22] Moreover, finer particles of GB carbide are more beneficial for GB strengthening and for inhibition of GB sliding and cracking.[1,2] Additionally, the fractographic analysis shows that the cracks not only occur along the GB,
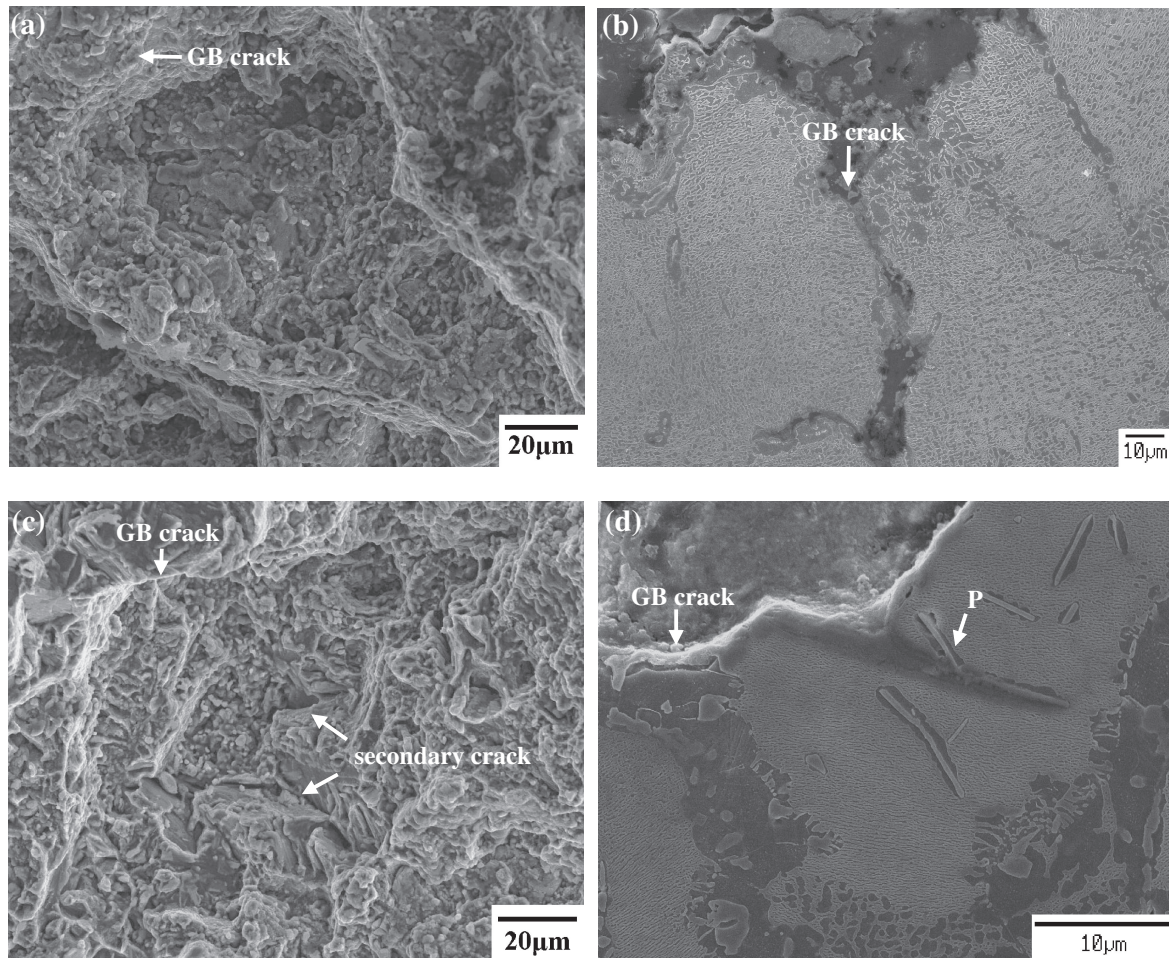
Fig. 9   SEM fractographs of 982°C/200 MPa creep test: (a) fracture surface and (b) longitudinal section of alloy A; (c) fracture surface and (d) longitudinal section of alloy D(5Re).

but also initiate and propagate along the P/γ interface or at the P phase in the alloy D(5Re), indicating that the presence of the needle-liked P phase increases likelihood of another source of crack. Moreover, the formation of P phases results in a decrease in solution-strengthening metal contents (e.g. W and Re) within the matrix. As discussed above, an optimum Re content of 3 mass% provides optimum tensile properties between conflicting factors of GB strength, γ' size, strength of γ matrix, and P phase.

4.2   Effect of Re on the creep behavior and micro-structural evolution

At high temperature, creep behavior was also determined by γ' size, strength of γ matrix, and GB strength. Most studies show that a cuboidal γ' with a size of ~0.1–0.5 μm, provides the best creep strength.[23,24] In this study, the amount of primary cuboidal γ' phase, of optimum particle size, increased with an increase in the content of Re, to benefit of creep strength. However, adding excessive Re to the alloy, as the alloy D(5Re), caused an in-homogeneous distribution of γ' phase. The large γ' phase (1–3 μm in size) existing in the region near the GB was detrimental to creep strength. On the other hand, most studies have reported large atomic radius Re partitions heavily to the γ matrix, increasing γ/γ' lattice misfit and strength of γ matrix, thereby hindering

dislocation motion, resulting in an improvement in creep strength.[9,25] Additionally, the evolution of γ' rafting was another major factor in determining creep behavior under high-temperature/low-stress conditions. The γ/γ' lattice misfit has a tendency to form cuboidal γ' phases, whereas a spherical γ' phase was observed for a near-zero γ/γ' lattice misfit.[26] The negative γ/γ' lattice misfit, caused by Re partitions in the γ matrix, provided the driving force for the formation of γ' rafts perpendicular to applied tensile stress.[26] The γ' rafting impeded the creep deformation by reducing the number of vertical (parallel to the direction of stress) γ channels.[27] It has been reported that γ' rafts are formed in the early stages of high temperature creep deformation, preventing dislocations to glide or climb.[27,28] Furthermore, narrower γ' raft spacing is more resistant to dislocation movement.[27] In this study, the γ' raft microstructure provided evidence that the development of γ' rafts has already finished in the early stages of creep (Fig. 10(d)), and that γ' raft spacing tended to decline with an increase in Re content in the alloy (Figs. 10(a)–(c)). Although alloy D(5Re) showed a well-developed γ' raft microstructure in the core area of the grain, the large γ' phase existing near the GB was detrimental to creep. The large γ' phases made it difficult for γ' rafts to form, due to their near spherical shape with a near-zero γ/γ' lattice misfit.[26] It must be emphasized that the secondary γ'
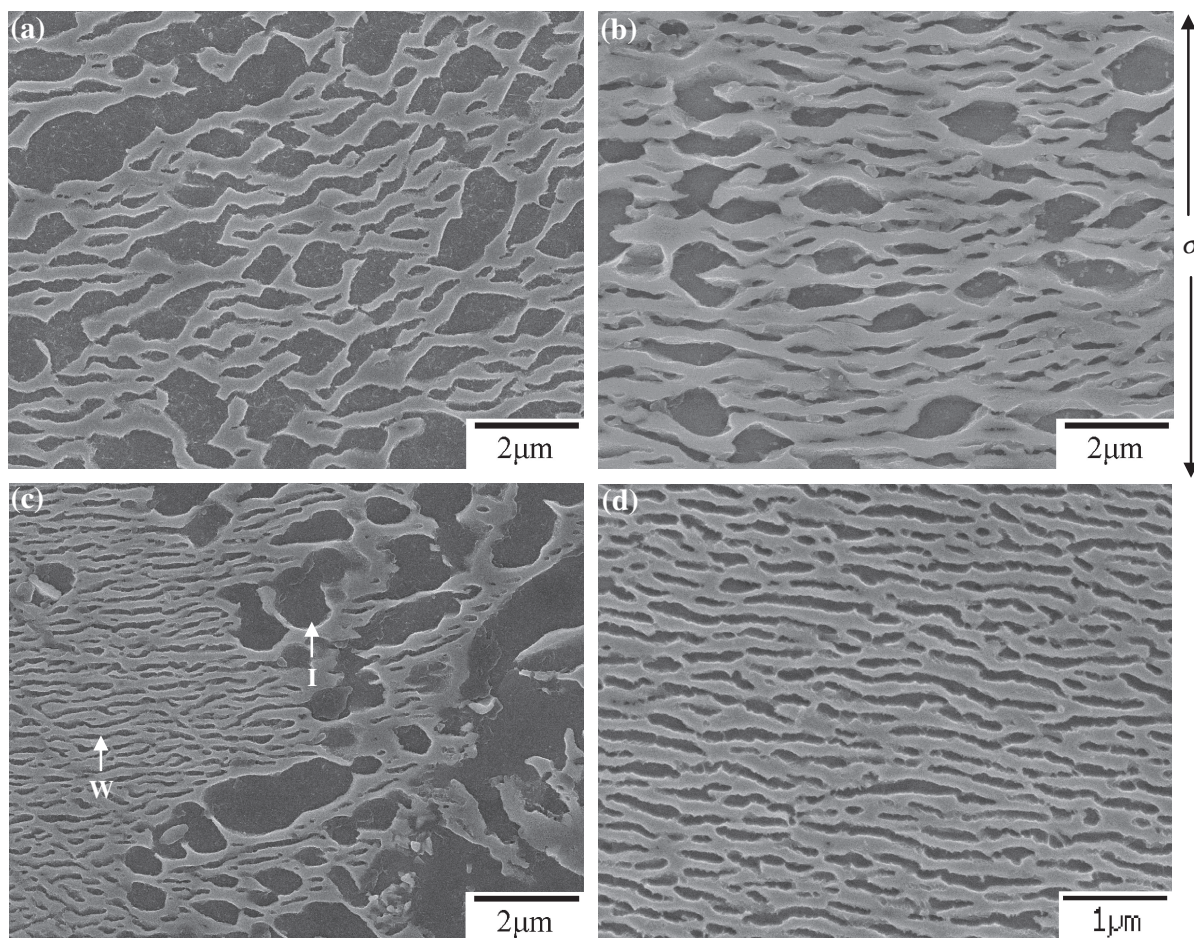
Fig. 10 γ' rafting microstructure of alloys (a) A, (b) C(3Re), and (c) D(5Re) in crept failure sample. For alloy D(5Re), the well-developed γ' raft exited in core area of grain marked as "W" and immature γ' raft existed near the GB marked as "I". (d) γ' rafting microstructure (in core area of grain) of alloy D(5Re) in interrupted creep specimens which were crept for 10 h.

phase was too small to resist the movement of dislocation. Moreover, the secondary γ' phase dissolved during creep. Therefore, the primary γ' played a more important role than the secondary γ' as a determinant of creep strength. In summary, a decrease in steady-state strain rate with Re content up to 3 mass%, suggests that optimizing Re addition could improve steady-state creep resistance by inhibiting the movement of dislocation in three ways: (1) increasing the amount of primary cuboidal γ' phase, (2) increasing strength of γ matrix, and (3) promoting development of γ' rafts.

In creep tests, strain hardening was opposed by increases in the stress associated with a reduction in cross-sectional area, and by recovery (due to dislocation climb and the subsequent annihilation of dislocations).[29,30] In this manner, the steady-state creep strain rate remained constant due to a balance among strain hardening, a reduction in the cross-section of the specimens, and recovery. In this study, 0~3 mass% Re-containing alloys showed steady-state creep regimes in the early stages of creep; however, alloy D(5Re) showed a continuing increase in creep rate, indicating that strain hardening was too low to counter the decrease in the cross-section of the specimen and recovery. The reduction in strain hardening was due to the P phase depleting the solid solution strengthening elements from the γ matrix and to the large γ' phase with immature γ' rafts that existed near the GB. The

result was a continuing increase in creep rate seen in the early creep stage of alloy D(5Re). It was noticed that more than approximately 1% strain in any of the alloys, accelerated the strain rate to failure. During this accelerated creep stage, a remarkable reduction in the cross-sectional area of the specimens resulted in a continual increase in the stress of the gage section, and consequent acceleration in the strain rate to failure. It has been proven that highly localized deformation in the vicinity of the fracture surface is responsible for a rapid increase in creep strain rate.[27] Thus, once the critical strain has been reached, the necking phenomenon dominates the behavior of accelerating creep stage. In our research, most of the cracks existed in the necked zone. This was evidence that the cracks probably initiated and propagated during the accelerating creep stage. Intergranular fractures occurred in the alloys containing 0~3 mass% Re, and the period of the accelerating creep increased with the content of Re up to 3 mass%, indicating that Re addition was sufficient to prevent cracks from propagating at the GB. It is interesting to note that the creep life, even the period of accelerating creep stage, was not reduced by grain refinement as Re content was increased to 3 mass%. The reason was that the presence of small and dense GB carbides prevented cracks from growing along the GB, resulting in an extension of the accelerating creep stage and creep life. Fractographic

observations showed that, for alloy D(5Re), the cracks were along the GB and along the P/γ interface—adding another source for carking. The needle-like P phase acts as a barrier for moving dislocations. Dislocations accumulated easily along the P/γ interface, leading to incoherence, and causing the appearance of interfacial cracking.[25] Therefore, the presence of the needle-liked P phase accelerates creep to fracture.

5. Conclusions

The following conclusions can be drawn from this work:
(1) Quantitative statistical analysis showed a decrease in the size of GB carbides and an increase in the number of GB carbides as Re content in Mar-M247 was increased. This GB carbide evolution is conducive to the promotion of GB strength.
(2) The tensile tests showed that both *UTS* and *YS* increased with an increase in Re content up to a maximum of 3 mass%. The small and dense GB carbides prevented the propagation of cracks contributing to the improvement of tensile strength. A decrease in tensile properties of alloy containing 5 mass% Re was caused by the formation of needle-like P phase.
(3) The 982°C/200 MPa creep tests showed that creep life increased with an increase in Re content up to a maximum of 3 mass%. The creep life of alloys with 3 mass% Re was extended by 2–3 times that of Re-free alloy. Adding 1∼3 mass% Re reduced the steady-state creep rate and postponed the onset of the acceleration stage in three ways: (1) increasing the amount of primary cuboidal γ' phase, (2) increasing strength of γ matrix, and (3) promoting the development of γ' rafts. An increase in the duration of the accelerated creep stage was caused by small and dense GB carbides preventing cracks from propagating along the GB, resulting in the prolongation of the accelerating creep stage. The above mentioned factors resulted in a prolongation of creep life. The formation of needle-like P phase, which increased creep rate to failure, was the major cause of the degradation of creep properties in alloy D(5Re).
(4) Cracks initiated and propagated along the GB in Mar-M247 superalloys with 0∼3 mass% added Re in tensile and creep tests. Cracks initiated and propagated along both the GB and P/γ interface in alloy D(5Re).

REFERENCES

1) H. Y. Bor, C. G. Chao and C. Y. Ma: Metall. Trans. A **30A** (1999) 551–561.
2) H. Y. Bor, C. G. Chao and C. Y. Ma: Scr. Meter. **38** (1998) 329–335.
3) W. F. Brown and S. J. Setlak: *Aerospace structural Metals Handbook*, thirty ninth ed., Vol. 6, Code 4218, (1999).
4) H. E. Huang and C. H. Koo: Mater. Trans. **45** (2004) 554–561.
5) C. N. Wei, H. Y. Bor and L. Chang: Mater. Trans. **49** (2008) 193–201.
6) Allied-Signal Aerospace Company, Garrett Engine Division, Specification No. EMS52508, (1991).
7) J. Rüusing, N. Wanderka, U. Czubayko, V. Naundorf, D. Mukherji and J. Rösler: Scr. Meter. **46** (2002) 235–240.
8) F. Diologent and P. Caron: Mater. Sci. Eng. A **385** (2004) 245–257.
9) K. Durst and M. Göken: Mater. Sci. Eng. A **387–389** (2004) 312–316.
10) G. E. Fuchs: Mater. Sci. Eng. A **300** (2001) 52–60.
11) M. V. Acharya and G. E. Fuchs: Mater. Sci. Eng. A **381** (2004) 143–153.
12) S. Wöllmer, T. Mack and U. Glatzel: Mater. Sci. Eng. A **319–321** (2001) 792–795.
13) A. F. Giamei and D. L. Anton: Metall. Trans. A **16A** (1985) 1997–2005.
14) R. Bürgel, J. Grossmann, O. Lüsebrink, H. Mughrabi, F. Pyczak, R. F. Singer and A. Volek: *Superalloy 2004*, (TMS, Warrendale, PA, 2004) pp. 25–34.
15) C. M. F. Rae and R. C. Reed: Acta Metall. **49** (2001) 4113–4125.
16) J. X. Yang, Q. Zheng, X. F. Sun, H. R. Guan and Z. Q. Hu: Mater. Sci. Eng. A **465** (2007) 100–108.
17) L. Liu, T. Huang, Y. Xiong, A. Yang, Z. Zhao, R. Zhang and J. Li: Mater. Sci. Eng. A **394** (2005) 1–8.
18) A. C. Yeh and S. Tin: Metall. Trans. A **37A** (2006) 2621–2631.
19) C. T. Sims, N. S. Stoloff and W. C. Hagel: *Superalloys II*, (John Wiley & Sons, New York, 1987) pp. 221–226.
20) A. Volek, R. F. Singer, R. Buergel, J. Grossmann and Y. Wang: Metall. Trans. A **37A** (2006) 405–410.
21) Allied-Signal Aerospace Company, Garrett Engine Division, Specification No. EMS55447, (1988).
22) C. T. Sims, N. S. Stoloff and W. C. Hagel: *Superalloys II*, (John Wiley & Sons, New York, 1987) pp. 91–95.
23) C. T. Sims, N. S. Stoloff and W. C. Hagel: *Superalloys II*, (John Wiley & Sons, New York, 1987) pp. 255–261.
24) J. S. Hou and J. T. Guo: J. Mater. Eng. Perform. **15** (2006) 67–75.
25) C. T. Sims, N. S. Stoloff and W. C. Hagel: *Superalloys II*, (John Wiley & Sons, New York, 1987) pp. 62–63.
26) L. J. Carroll, Q. Feng, J. F. Mansfield and T. M. Pollock: Metall. Trans. A **37A** (2006) 2927–2938.
27) R. C. Reed, N. Matan, D. C. Cox, M. A. Rist and C. M. F. Rae: Acta Mater. **47** (1999) 3367–3381.
28) A. C. Yeh, A. Sato, T. Kobayashi and H. Harada: Mater. Sci. Eng. A **490** (2008) 445–451.
29) R. E. Reed-Hill and R. Abbaschian: *Physcial Metallurgy Principles*, (PWS Publishing Company, Boston, 1994) pp. 881–885.
30) L. Z. He, Q. Zheng, X. F. Sun, H. R. Guan, Z. Q. Hu, A. K. Tieu, C. Lu and H. T. Zhu: Metall. Trans. A **36A** (2005) 2385–2391.